Supporting Information

Giant Resistive Switching in Mixed Phase BiFeO₃ via phase population control

David Edwards[1,□], Niall Browne[1,□], Kristina M. Holsgrove[1], Aaron B. Naden[1], Sayed O. Sayedghaee[2], Bin Xu[3], Sergey Prosandeev[3], Dawei Wang[4], Dipanjan Mazumdar[5], Martial Duchamp[6,7], Arunava Gupta[8], Sergei V. Kalinin[9], Miryam Arredondo[1], Raymond G. P. McQuaid[1], Laurent Bellaiche[3], J. Marty Gregg[1], Amit Kumar[1*]

[1]School of Mathematics and Physics, Queen's University Belfast, Belfast, BT7 1NN, United Kingdom
[2]Microelectronics-Photonics Program and Physics Department, University of Arkansas, Fayetteville, Arkansas 72701, USA
[3]Physics Department and Institute for Nanoscience and Engineering, University of Arkansas, Fayetteville, Arkansas 72701, USA
[4]Electronic Materials Research Laboratory, Key Laboratory of the Ministry of Education and International Center for Dielectric Research, Xi'an Jiaotong University, Xi'an 710049, China
[5]Department of Physics, Southern Illinois University, Carbondale, Illinois 62901, USA
[6]Ernst Ruska Centre for Microscopy, Forschungszentrum Juelich, Juelich 52428, Germany
[7]School of Materials Science and Engineering, Nanyang Technological University, Singapore 639798, Singapore
[8]Center for Materials for Information Technology, University of Alabama, Tuscaloosa, Alabama 35487, USA
[9]Center for Nanophase Material Sciences, Oak Ridge National Laboratory, Oak Ridge, Tennessee, 37831, USA

*Corresponding author: a.kumar@qub.ac.uk

□ These authors contributed equally to the work.

This document provides additional details on the structural characterization of the stress induced conductive interfaces in mixed phase BiFeO₃, reversible switching of mixed phase populations using stress and electrical bias, theoretical modeling of the phase competition under applied stimuli, details of experimental analysis which enable comparison of the theoretical calculations with experimental data, and data illustrating retention and cyclability of the resistance states during microprobe based resistive switching.

1. Structural investigation of strain mediated origin of conduction in stress induced R/T boundaries : Scanning Transmission Electron Microscopy (STEM) characterization of the epitaxial nature of the studied BFO film has been undertaken. **Figure S1** shows a cross-section of the BFO film acquired along the $[010]_{pc}$ direction and the excellent registry of the film with respect to the substrate is demonstrated. These data confirm the epitaxial nature of the BFO film where the as-grown T-phase shows an in-plane lattice parameter of 0.371 nm in comparison to the in-plane pseudocubic lattice constant of 0.379 nm for the substrate

LAO. These values are consistent with values of lattice constants of T-phase films reported using TEM/XRD in the existing literature [1,2].
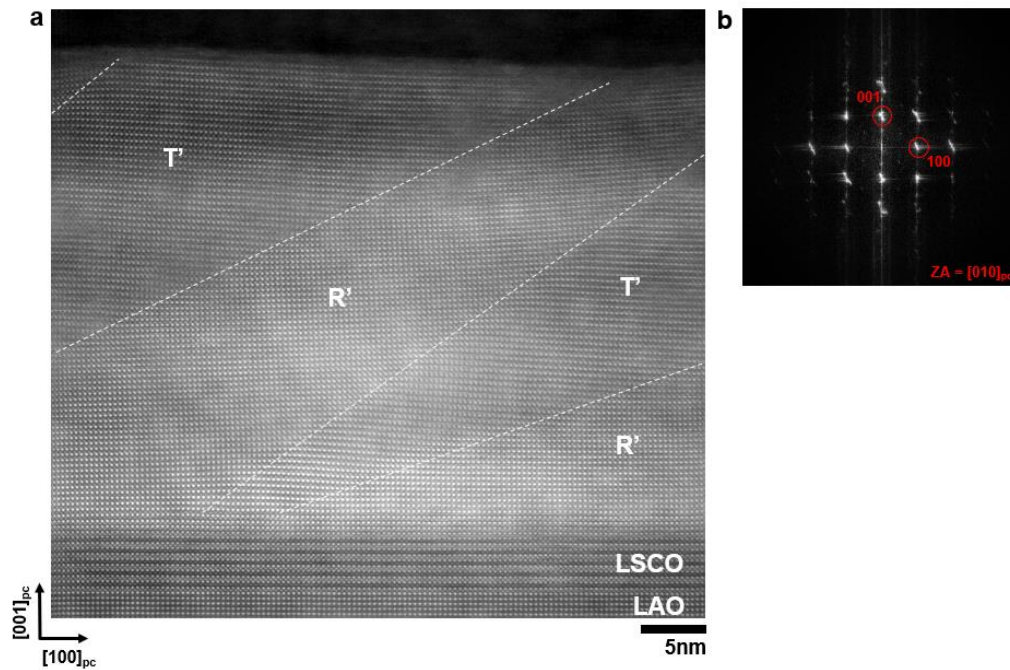

Figure S1. STEM characterisation of the epitaxial BFO thin film (a) STEM HAADF image showing a stress-written mixed-phase region within a cross-section of the BFO thin film, acquired along the $[010]_{pc}$ direction. The LAO substrate and LSCO electrode are labelled. White dashed lines are associated with the boundaries which separate the stress-written R' and T' phases within the BFO thin film. (b) Diffractrogram taken by FFT of the HAADF image confirms the high-quality nature of the epitaxially grown BFO thin film. The spots from the lattice planes along the out-of-plane 001_{pc} and in-plane 100_{pc} reciprocal space directions demonstrate splitting due to the variation in lattice parameters between LAO, LSCO, R' phase and T' phase BFO, in agreement with previous characterisation reports [1, 3-5].

In order to investigate potential structural changes at the pressure-written R/T boundaries and their impact on the film's functional properties, cross-sections from regions of the as-grown and pressure-written film were analyzed using scanning transmission electron microscopy (STEM) as shown in **Figs. S2**a and S2b, respectively. Nanobeam electron diffraction (NBED) was used to locally map the in-plane crystallographic deformation of the BFO film across the interfaces between the R- and T-phases, the results are shown in Figs. S2c and S2d. To highlight the differences in lattice spacing at the interfaces, Figs. S2c and S2d show the gradient of the deformation of the BFO films with respect to the unstrained LAO substrate along the horizontal axis of the images, i.e. $\nabla.\epsilon_{xx} = \nabla.([d_{LAO} - d_{BFO}]/d_{LAO})$. Corresponding line profiles are shown in Figs. S2e and S2f, respectively. These data reveal a notable enhancement of $\nabla.\epsilon_{xx}$ at the interfaces in the pressure-written region with average values of $\sim 8 \times 10^{-3}$ nm^{-1} compared to $\sim 5 \times 10^{-3}$ nm^{-1} in the as grown film. This therefore

suggests that the interfaces in the pressure-written regions of the film are significantly more abrupt with rapid changes in the in-plane crystallography between the two phases.
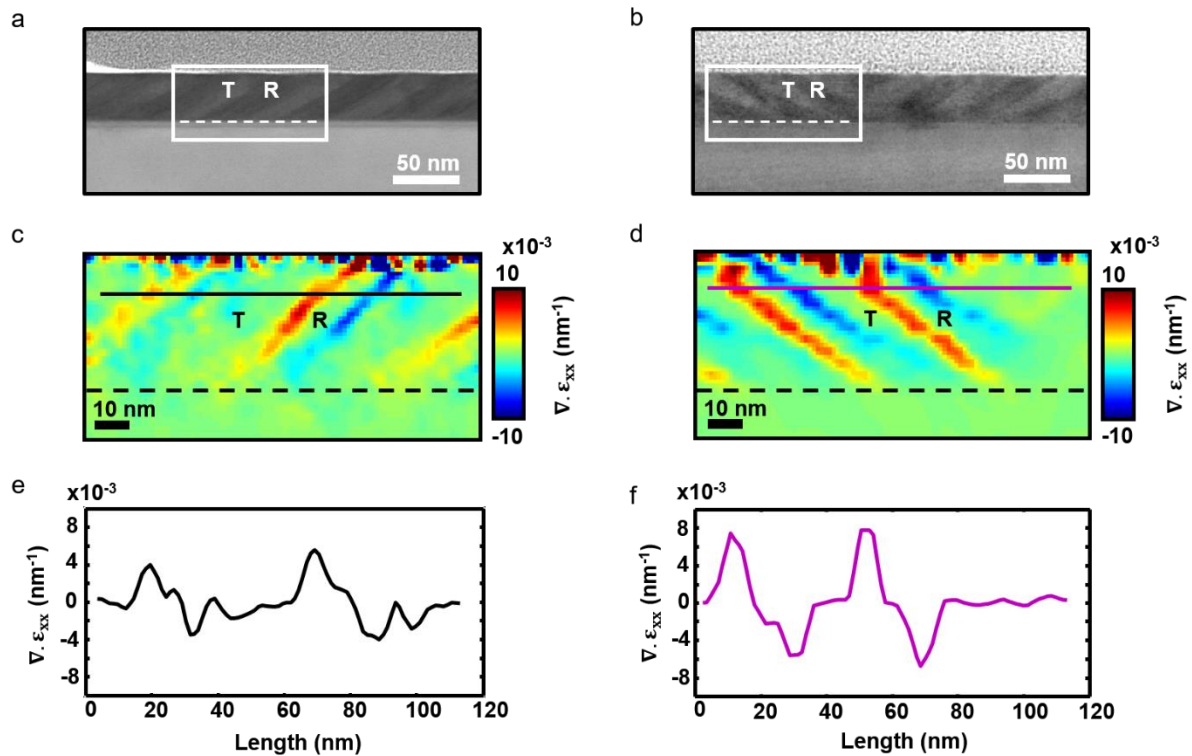

Figure S2. Structural investigation of strain mediated origin of conduction in stress induced R/T boundaries (a,b) Cross-sectional STEM images from as grown and stress-written regions of the film, respectively. The R-phase needles are embedded in the T-phase matrix, as shown by the annotations. (c,d) Corresponding maps of the in plane strain gradient, $\nabla . \varepsilon_{xx}$. Their line profiles are shown in (e,f) and highlight increased strain gradients at the R/T interfaces in the stress-written film. The increased gradients at the newly formed R needles coincide with increased conduction observed around them.

It has previously been rationalized that the bandgap in BFO is controlled by the degree of O 2p and Fe 3d orbital overlap and hence by the Fe—O—Fe bond angle[6,7]. Therefore, rapid changes of the unit cell – as observed from the increased $\nabla . \epsilon_{xx}$ at the R/T interfaces here – can lead to increased orbital overlap by a straightening of the aforementioned bond angle and thus a reduction of the bandgap.

Another possibility is migration of O vacancies to the interfaces, introducing energy states into the bandgap[8]. However, this is unlikely here since the structural transitions are reversible (such defects would likely pin switching and transitions) and multiple cycles do not cause degradation of the functional properties unlike the fatigue observed in other mixed phase systems such as $PbZrTiO_3$. We therefore rationalize the enhanced conductivity as arising from the increased $\nabla . \epsilon_{xx}$ at the pressure-written interfaces.

2. Piezoresponse force microscopy study of dual control method

In the main text, a dual control method was established where electric field drives the phase of an epitaxially strained BFO thin film towards the T phase and uniaxial stress towards the R phase. In **Figure S3** and **Figure S4**, we demonstrate this dual control method through a series of piezoresponse force microscopy (PFM) images. Figure S3 displays the same example used in the main text, accompanied by vertical PFM amplitude and phase images demonstrating the switching in the out-of-plane phase of the film under electric field and the resulting amplitude contrast by the mechanically-induced needle-like structures. This highlights that the needle-like structures correspond to R phase ferroelectric domains with a comparable PFM response to the pre-existing R phase needles. This is further highlighted in Figure S4 through another example where the topography is accompanied by both the vertical and lateral PFM signal ($A\cos\theta$, where A corresponds to the PFM amplitude and θ the PFM phase).
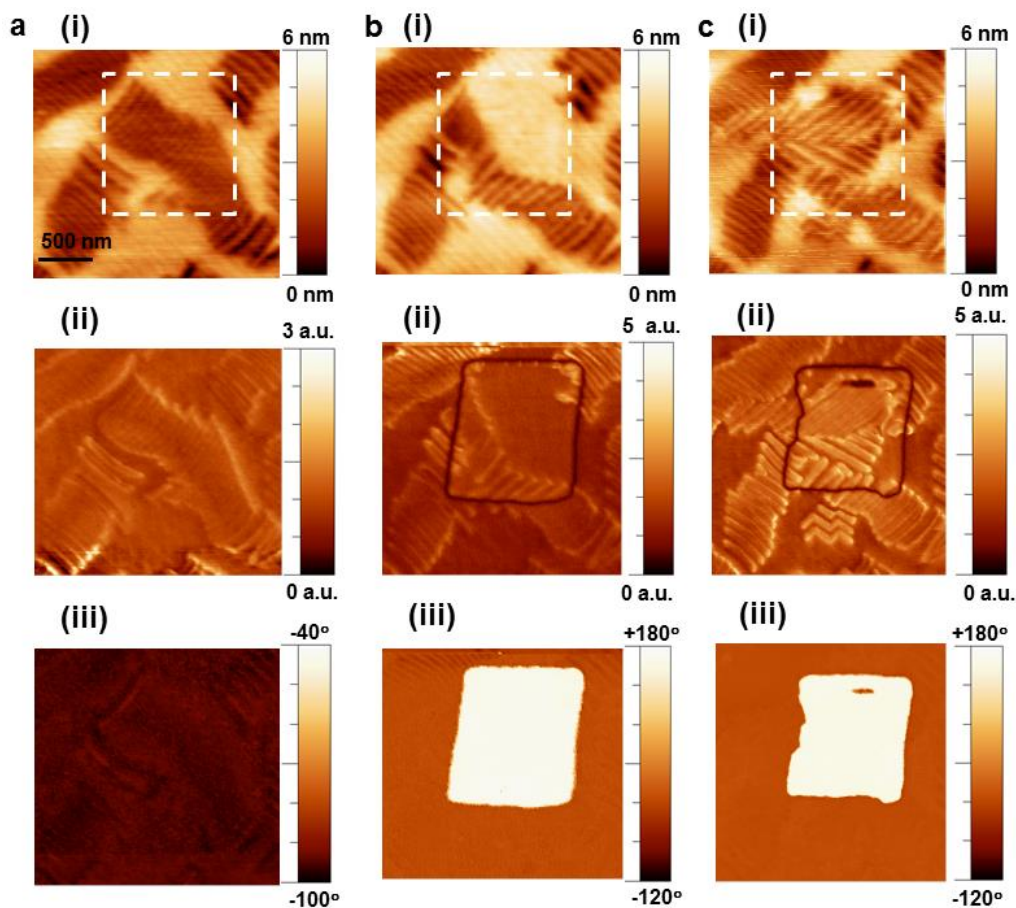

Figure S3. PFM imaging of stress and electric field dual control method. (a) (i) Initial topography, vertical PFM (ii) amplitude and (iii) phase. (b) After application of electric field to region demarcated by dashed line. (c) After application of mechanical stress.
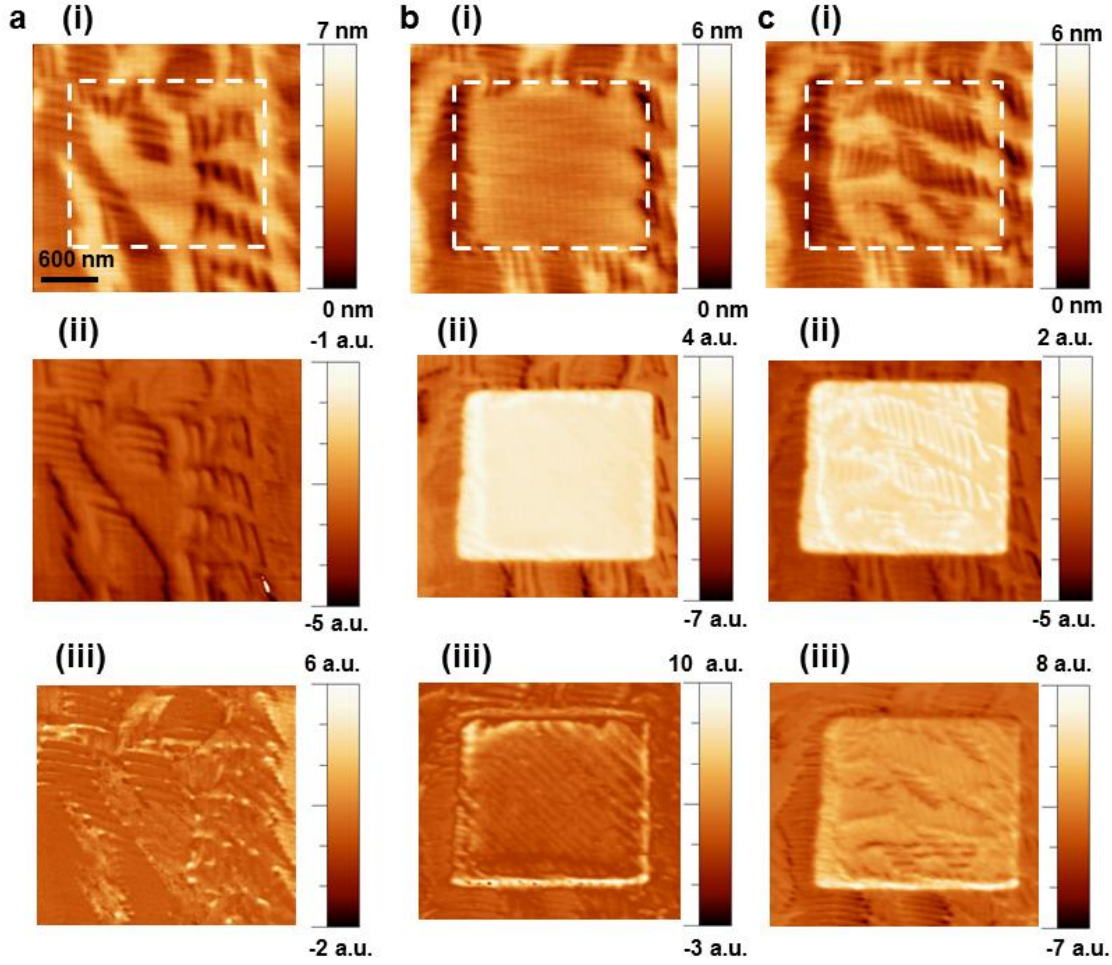
Figure S4. (a) (i) Initial topography, (ii) vertical PFM signal and (iii) lateral PFM signal. (b) After application of electric field to region marked by dashed line and (c) after application of mechanical stress.

3. Three dimensional scatter plot of predicted population of R phase

As mentioned in the main text, the mechanical lever rule was applied to the effective Hamiltonian energy calculations in order to obtain predictions on the relative proportion of R phase (x_R) and T phase (x_T) in the BFO film as a function of misfit strain (S_i). In the form of the lever rule used in this work and shown again below, S_T and S_R are the strains at which the common tangent intercepts the T phase and R phase energy curves respectively

$$S_i = x_T S_T + x_R S_R \qquad \text{(S1)}$$

As shown in **Figure S5**, the intercepts represent the limiting cases where at larger compressive strains than S_T, $x_T = 1$, while at smaller compressive strains than S_R, $x_R = 1$. At any strain S_i along the tangent, equation S1 can be re-arranged as follows to enable determination of x_R (chosen arbitrarily to x_T), knowing that x_R and x_T sum to unity

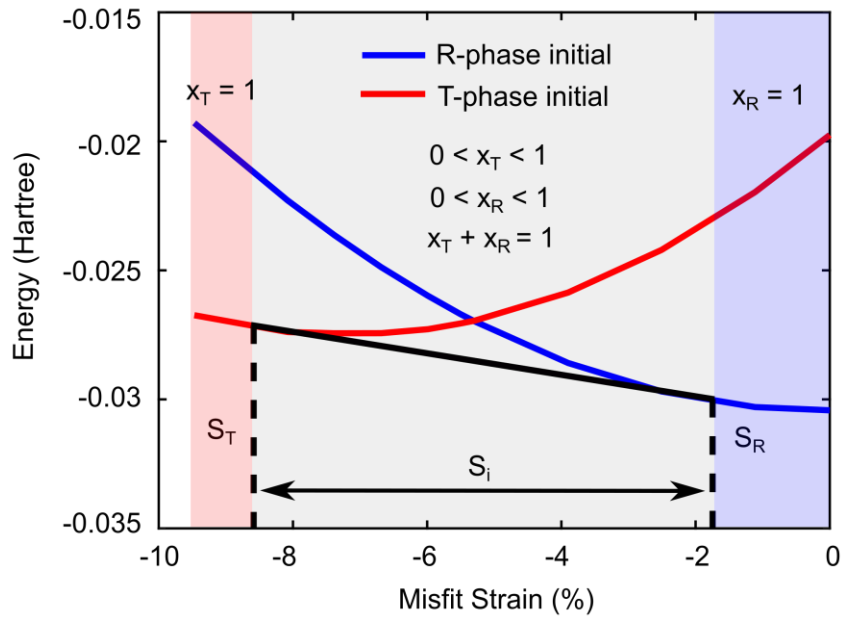$$x_R = \frac{S_i - S_T}{S_R - S_T} \qquad \text{(S2)}$$

Figure S5. Illustration of the common tangent drawn between plots of energy as a function of misfit strain for the R phase and T phase under no applied stress or electric field.

x_R was subsequently calculated at a series of different S_i values and the process repeated for a large range of energy curves simulated under various combinations of stress and electric field. This resulted in the discretized 3D scatter plot of the predicted % population of R phase (**Figure S6**) as function of three variables: electric field, stress and misfit strain. The linear relationship evident between each variable and the phase population in the film permitted linear interpolation of the predicted populations along each axis. Plotting the continuous, interpolated data (via Matlab) generated the graphical representations shown in the main text.
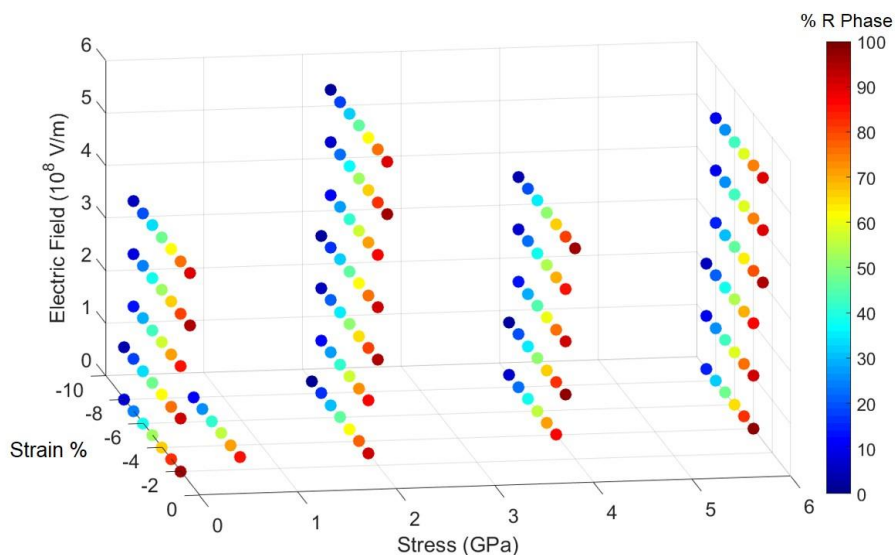

Figure S6. Scatter plot of the predicted population of R phase (color) as a function of misfit strain, electric field and uniaxial stress.

4. Experimental phase population map and calculation details

Figure S7 demonstrates the enlarged topography containing the grid experiment carried out to obtain a direct experimental comparison to the theoretical predictions. In order to subsequently calculate the change in the population of the R and T phase, a numerical analysis of the topography surface was carried out. Each topography image consists of pixels corresponding to a height value and due to the fact that the height is indicative of the phase structure a critical height was set, above which the film is considered T phase, or conversely R phase below. The fraction of pixels above and below the critical height was subsequently calculated enabling a numerical estimation of the phase population in the film.
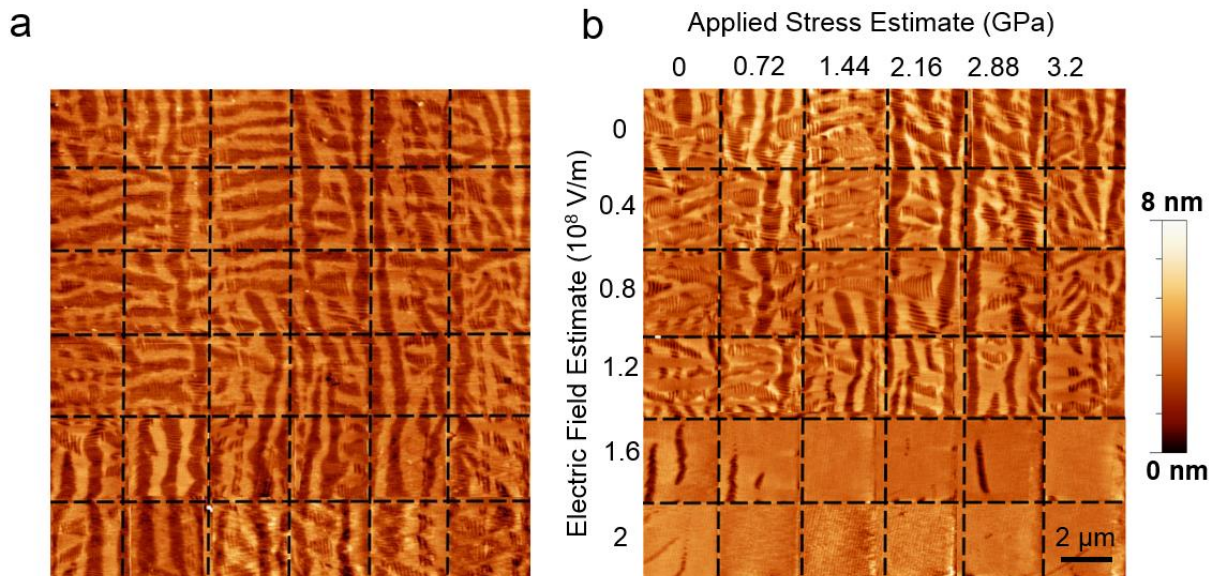

Figure S7. Grid experiment carried out to construct a map of the change in phase population with varying uniaxial stress and electric field. (a) Topography before and (b) after the application of varying uniaxial stresses, electric fields and simultaneously applied combinations of both.

5. Retention and cyclability of the resistance states during microprobe based resistive switching

In the microprobe based resistive measurements, we have tested the retention of two different capacitors driven into the conductive state (via macroscopic stress) and resistive state (via bias) intermittently over a period of ~ 11 days. The results are shown in **Figure S8** and suggest that the two states are quite robust over time. There appears to be no meaningful reduction in the difference between the two states in terms of conductance.
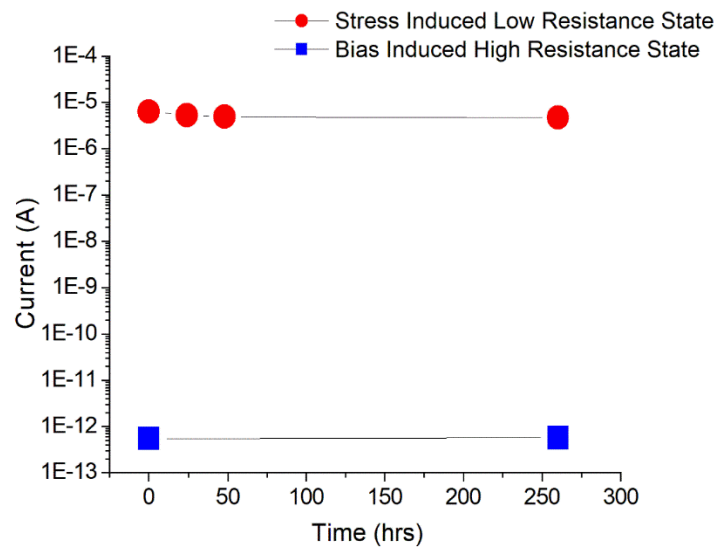
Figure S8. Retention (at room temperature) of the conducting and resistive states in macroscopic resistive measurements taken over several days. Current observed in a stress-induced conducting state under a capacitor at t = 0, 24, 48 and 260 hrs is shown in red circles while current observed in a bias-induced resistive state under a different capacitor at t = 0 and 260 hrs is shown in blue squares. All currents were measured at 2V.
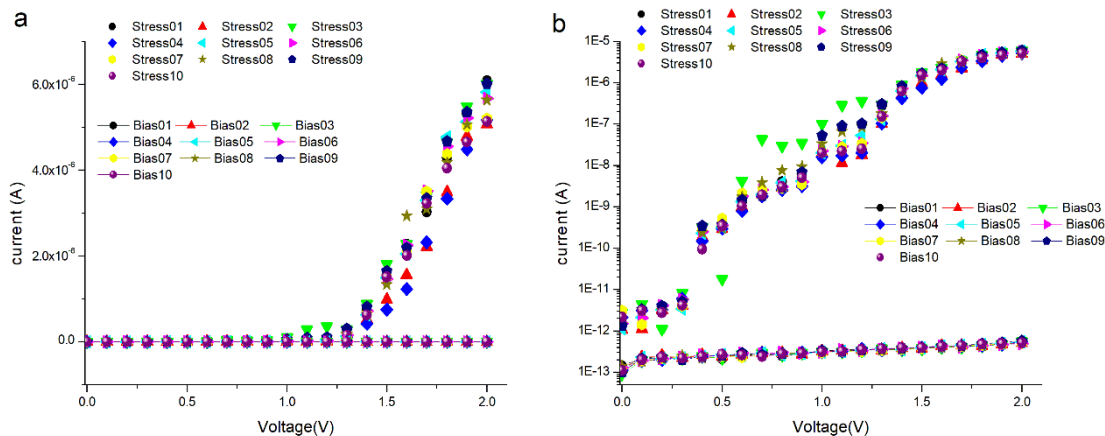

Figure S9. Endurance (at room temperature) of the conducting and resistive states over 10 cycles in macroscopic probe-based resistive switching measurements (a) I-V behaviour observed in the stress-induced conducting and bias-induced resistive states taken over 10 consecutive cycles (b) data shown using a logarithmic current scale. The scatter plots (labelled Stress01-Stress10) show the I-V behaviours of the stressed capacitor (conductive state) after each switching event, while the line-scatter plots (labelled Bias01-Bias10) show the I-V behaviours after the application of each electrical bias switching event, which drives the material into the resistive state.

In the macroscopic measurements, we have attempted to demonstrate cyclability between the stress-induced conducting and bias-induced resistive states over several cycles. In the original manuscript, we have shown such data over three cycles. In follow-up studies, we achieved further cyclability with data shown in **Figure S9** over 10 cycles. The data shows good repeatable switching and there is no restriction, from the material perspective, in terms of repeatability of the switching. In our attempts to examine further mapping beyond 10-20 cycles, we have found that the electrode lifetime is limited, as our current microprobe setup used to apply stress degrades the electrodes through scratching and delamination. For future work, we are seeking to optimise the electrodes and to develop an automated stress system that could allow very precise graduated control of the applied stress in the macroscopic measurements as this would minimise top electrode degradation.

6. Enhanced local conduction profiles (averaged over several lines) with increasing levels of AFM tip pressure: Different regions of the BFO film were manipulated with increasing levels of stress and averaged current profiles over the regions showed an increasing trend (**Figure S10**). This could arise due to increased number of new conducting R/T interfaces as well as enhanced conductivity of the interfaces themselves.
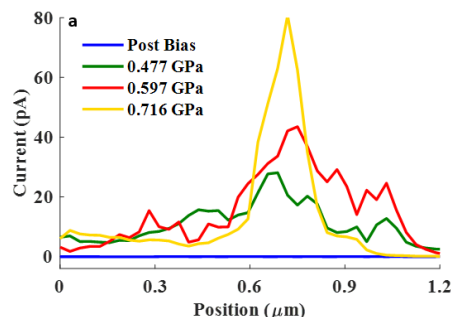

Figure S10. Enhanced averaged local conduction profiles observed in AFM based experiments with increasing levels of applied stress via tip.

References

[1] R. J. Zeches, M. D. Rossell, J. X. Zhang, A. J. Hatt, Q. He, C. H. Yang, A. Kumar, C. H. Wang, A. Melville, C. Adamo, G. Sheng, Y. H. Chu, J. F. Ihlefeld, R. Erni, C. Ederer, V. Gopalan, L. Q. Chen, D. G. Schlom, N. A. Spaldin, L. W. Martin and R. Ramesh, *Science*, 2009, **326**, 977-980.

[2] D. Mazumdar, V. Shelke, M. Iliev, S. Jesse, A. Kumar, S. V. Kalinin, A. P. Baddorf and A. Gupta, *Nano Lett.*, 2010, **10**, 2555-2561.

[3] M. D. Rossell, R. Erni, M. P. Prange, J. C. Idrobo, W. Luo, R. J. Zeches, S. T. Pantelides and R. Ramesh, *Phys. Rev. Lett.*, 2012, **108**, 047601.

[4] J. X. Zhang, X. X. Ke, G. Y. Gou, J. Seidel, B. Xiang, P. Yu, W. I. Liang, A. Minor,

Y. H. Chu, G. Van Tendeloo, X. B. Ren and R. Ramesh, *Nat. Commun.*, 2013, 4, 2768.

[5] J. X. Zhang, R. J. Zeches, Q. He, Y. H. Chu and R. Ramesh, *Nanoscale*, 2012, 4, 6196-6204.

[6] J. Seidel, M. Trassin, Y. Zhang, P. Maksymovych, T. Uhlig, P. Milde, D. Kohler, A. P. Baddorf, S. V. Kalinin, L. M. Eng, X. Q. Pan and R. Ramesh, *Adv. Mater.*, 2014, **26**, 4376-4380.

[7] G. Catalan and J. F. Scott, *Adv. Mater.*, 2009, **21**, 2463-2485.

[8] M. Brazier, S. Mansour and M. McElfresh, *Appl. Phys. Lett.*, 1999, **74**, 4032-4033.